Polarization behavior of elastic scattering from a silicon microsphere coupled to an optical fiber

Mohammed Sharif Murib,[1] Emre Yüce,[1] Oğuzhan Gürlü,[2] and Ali Serpengüzel[1,*]

[1]*Koç University, Microphotonics Research Laboratory, Department of Physics, Rumelifeneri Yolu, Sarıyer, Istanbul 34450, Turkey*

[2]*Istanbul Technical University, Faculty of Sciences and Letters, Department of Physics, Maslak, Sarıyer, Istanbul 34469, Turkey*

**Corresponding author: aserpenguzel@ku.edu.tr*

Received December 18, 2013; revised January 22, 2014; accepted January 22, 2014; posted January 23, 2014 (Doc. ID 201702); published February 19, 2014

The polarization behavior of elastic scattering at 1473 nm is analyzed from a silicon microsphere on an optical fiber half-coupler. The 0.27 nm angular mode spacing of the resonances correlates well with the optical size of the silicon sphere. The spectral linewidths of the resonances are on the order of 10^{-3} nm, which corresponds to quality factors on the order of 10^6. The transverse magnetically polarized elastic scattering signal has higher resonance to modulation depth and background ratio than the transverse electrically polarized elastic scattering signal and is suitable for high-resolution optical filtering applications such as optical monitoring and sensing. © 2014 Chinese Laser Press

OCIS codes: (130.3060) Infrared; (140.3945) Microcavities; (230.5750) Resonators; (290.5850) Scattering, particles; (290.5855) Scattering, polarization.

http://dx.doi.org/10.1364/PRJ.2.000045

1. INTRODUCTION

Silicon has excellent material properties such as high thermal and electrical conductivity and high optical damage threshold. In addition, silicon is relatively cheap and has high-volume manufacturability potential, leading to the realization of electronic and photonic integration through the silicon photonics [1] revolution for near-infrared [2] and mid-infrared [3] communication, as well as computation [4] and sensing [5,6] applications. Silicon with a bandgap of 1.1 eV is transparent in the near-infrared optical communication wavelengths, and optical fibers [7] and waveguides [8] with a silicon core have already been realized.

Circular cavities [9] such as microspheres [10], microdisks [11], microtoroids [12], and microrings [13] with high quality-factor resonances continue to motivate a high number of photonics researchers. The electromagnetic wave can be trapped inside a circle by almost total internal reflection [14]. After circumnavigating inside the circle, the optical wave returns back to its initial starting point in phase for specific wavelengths [15]. A periodic circumnavigation of the electromagnetic wave in the circle manifests itself as a series of sharp spectral peaks known as whispering gallery modes (WGMs) or morphology-dependent resonances. High-quality-factor WGMs of circular microcavities open up new perspectives in communication [16,17], sensing [18], light emission [19], and fundamental optics [20].

Silicon microspheres [21–23] and germanium microspheres [24] were studied for electronic and photonic integration applications. Silicon microspheres have been used for optical modulation applications in air [25] and in nematic liquid crystals [26]. Polarization switching [27] has been proposed, and polarization-discriminated transmission [28,29] and fluorescence [30] have been performed in silica microspheres.

In this study, we analyze the polarization behavior of the elastic scattering from a silicon microsphere in air placed on a silica optical fiber half-coupler (OFHC) and excited with a tunable near-infrared laser operating in the standard optical fiber communication band (S-band) for the first time to our knowledge.

2. MICROSPHERE PARAMETERS

Figure 1 shows the schematic of the silicon microsphere with radius **a** and relative refractive index m (with respect to the surrounding medium) coupled to a silica OFHC with its fiber core placed at an impact parameter b away from the microsphere center. The input Gaussian beam has transverse electric (TE) and transverse magnetic (TM) components defined with respect to the microsphere under excitation. The TE component of the polarization is *senkrecht* (s-polarized), that is, pointing outside the plane of the paper, while the TM component of the polarization is parallel (p-polarized), that is, in the plane of the paper (the scattering plane).

The spectral mode spacing $\Delta\lambda$ is the spectral spacing between the WGMs of same radial mode order ℓ and consecutive angular mode number n, which can be calculated by [31]

$$\Delta\lambda = \frac{\lambda^2 \tan^{-1}\rho}{2\pi a\rho}, \tag{1}$$

where λ is the vacuum wavelength of incoming light and $\rho = \sqrt{(m^2 - 1)}$.

The spectral density of all WGMs, which is the number N of all the WGMs including all polar angular mode numbers n and

 © 2014 Chinese Laser Press

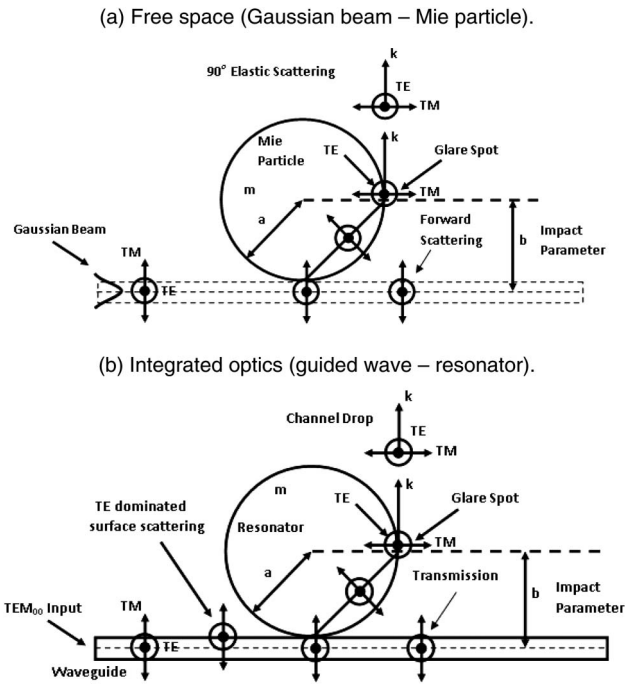


Fig. 1. (a) Free-space and (b) integrated optics depiction of a silicon microsphere with radius a coupled to a single-mode OFHC placed at an impact parameter b, and the elastic scattering due to the WGMs, GS, and SI.

all radial mode orders ℓ as a function of size parameter $x = 2\pi a/\lambda$, can be estimated by [32]

$$\frac{\mathrm{dN(x)}}{\mathrm{dx}} = \frac{\mathrm{x}\rho^2(\rho - \tan^{-1}\rho)}{\pi}. \tag{2}$$

The spectral density of all WGMs can be estimated as a function of wavelength as the following:

$$\frac{\mathrm{dN}(\lambda)}{\mathrm{d}\lambda} = \frac{4\pi \mathrm{a}^2\rho^2(\rho - \tan^{-1}\rho)}{\lambda^3}. \tag{2a}$$

However, once the wavelength λ of the excitation laser is resonant with the WGM, only the WGMs with the appropriate quality factor Q [33], the impact factor b [34], and the propagation constant k [35] will be excited by the incoming Gaussian beam in the single-mode OFHC.

For a spheroid, the degeneracy of the WGMs will be lifted, and the WGM angular frequencies will be [36]

$$\omega(\mathrm{m}) = \omega_o\left\{1 - \frac{e}{6}\left[1 - \frac{3\ m^2}{n(n+1)}\right]\right\}, \tag{3}$$

where ω_o is the degenerate WGM angular frequency, $e > 0$ the prolate ellipticity, $e < 0$ the oblate ellipticity, and m the azimuthal angular mode number, which is $2n + 1$ times degenerate. The corresponding WGM wavelengths will be

$$\lambda(m) = \lambda_o\left\{1 + \frac{e}{6}\left[1 - \frac{3\ m^2}{n(n+1)}\right]\right\}, \tag{3a}$$

where λ_o is the degenerate WGM wavelength. The maximum shift is observed for $m = n$:

$$\lambda(\mathrm{n}) = \lambda_o\left\{1 + \frac{e}{6}\left[1 - \frac{3n^2}{n(n+1)}\right]\right\}, \tag{3b}$$

whereas the minimum shift is observed for $m = 0$:

$$\lambda(0) = \lambda_o\left\{1 + \frac{e}{6}\right\}. \tag{3c}$$

Therefore the wavelength shift region is given by

$$\lambda(\mathrm{n}) - \lambda(0) = \lambda_o\left\{\frac{e}{2}\left[\frac{n}{(n+1)}\right]\right\}. \tag{3d}$$

The minimum spectral spacing of the degenerate WGMs can be estimated by dividing the wavelength shift region by the polar angular mode number n,

$$\frac{\lambda(\mathrm{n}) - \lambda(0)}{n} = \lambda_o\left\{\frac{e}{2}\left[\frac{n^2}{n(n+1)}\right]\right\}\frac{1}{n} = \frac{\lambda_o e}{2(n+1)}. \tag{4}$$

The OFHC is manufactured from a single-mode optical fiber with a core radius of $\omega_o = 2$ micrometers. The typical polar angular mode numbers n are on the order of the size parameter $x = 2\pi a/\lambda$. These degenerate modes will cover a polar angular distribution of $\pi/2$ radians. The polar angular coverage of the OFHC will correspond to ω_o/b radians, which in turn corresponds to $4a\omega_o/b\lambda$-fold WGM degeneracy. For excitation with a single-mode OFHC, the excitable WGM degeneracy decreases with increasing sphere radius.

3. ELASTIC SCATTERING INTENSITIES

The elastically scattered electric field has contributions from three sources: (1) the WGM electric field (E_{WGM}); (2) the refracted beam, that is, the glare spot (GS) electric field (E_{GS}); (3) and the OFHC surface imperfection (SI) scattered electric field (E_{SI}) [37]. The total elastically scattered electric field can then be written as

$$E_{\mathrm{total}} = E_{\mathrm{WGM}} + E_{\mathrm{GS}} + E_{\mathrm{SI}}, \tag{5}$$

and the total elastically scattered intensity can be written as

$$I_{\mathrm{total}} = \frac{c\varepsilon_o}{2}|E_{\mathrm{WGM}} + E_{\mathrm{GS}} + E_{\mathrm{SI}}|^2, \tag{6}$$

where c is the speed of light in vacuum and ε_o is the vacuum permittivity.

The interference of these elastically scattered electric fields contributes to the constant background (BG) and the slowly varying modulation depth (MD) observed in the elastic scattering signal represented in Fig. 2, which also illustrates the narrow linewidth WGMs and the spectral mode spacing ($\Delta\lambda$). The constant BG is the nonresonant "dc" value of the spectra. The narrow linewidth WGMs have Lorentzian line shapes on top of the slowly varying MD oscillating at $\Delta\lambda$.

In the 90° elastic scattering geometry, the SI term contributes more TE polarized elastic scattering signal than the TM polarized elastic scattering signal. Therefore, by neglecting the SI term for the TM polarization, the elastically scattered intensities can be written as

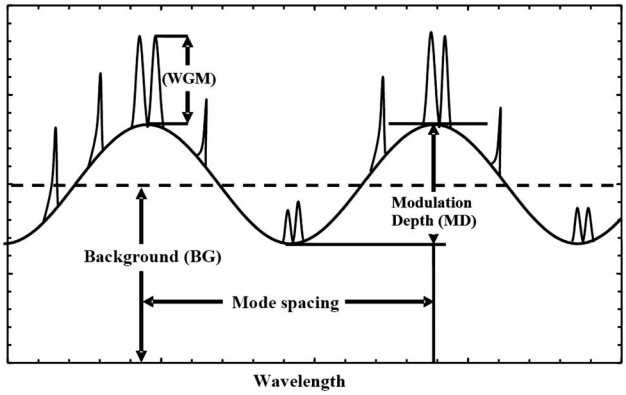


Fig. 2. Illustration of an elastic scattering spectrum from a microsphere indicating the WGMs, the MD, the BG, and the spectral mode spacing ($\Delta\lambda$).

$$I_{\text{total}} = \frac{c\varepsilon_o}{2}|E_{\text{WGM}} + E_{\text{GS}} + E_{\text{SI}}|^2 \tag{7TE}$$

$$I_{\text{total}} = \frac{c\varepsilon_o}{2}|E_{\text{WGM}} + E_{\text{GS}}|^2 \tag{7TM}$$

which gives

$$I_{\text{total}} = I_{\text{WGM}} + I_{\text{GS}} + I_{\text{SI}} + c\varepsilon_o|E_{\text{WGM}}E^*_{\text{GS}} + E_{\text{WGM}}E^*_{\text{SI}} + E_{\text{GS}}E^*_{\text{SI}}|, \tag{8TE}$$

$$I_{\text{total}} = I_{\text{WGM}} + I_{\text{GS}} + c\varepsilon_o|E_{\text{WGM}}E^*_{\text{GS}}|, \tag{8TM}$$

which should equal the elastic scattering intensities of the WGMs, BG, and MD:

$$I_{\text{total}} = I_{\text{WGM}} + I_{\text{BG}} + I_{\text{MD}}. \tag{9}$$

The comparison of Eqs. (8) and (9) shows that there are two contributions to the BG = GS + SI for the TE polarization, whereas there is only one contribution to the BG = GS for the TM polarization. For the TE polarization all of the three possible combinations of the WGM + GS + SI contribute to the MD, whereas for the TM polarization there is only one possible combination of the WGM + GS contributing to the MD. Therefore, for the TM polarization, there would be less BG and MD in the elastic scattering spectra.

The intensity of the WGMs should be on the same order of magnitude in the TE and TM polarized spectra. However, the intensity of the MD and the BG depend on the amount of extra scattered light, that is, SI + GS, available at that polarization.

4. EXPERIMENTAL SETUP

Figure 3 shows the schematic of the experimental setup. A tunable diode laser (DL) with a wavelength of 1473 nm is used in order to excite the WGMs of the silicon microsphere through a single-mode OFHC, which couples 99.4% of the light passing through the coupler when an index-matching oil is placed on the OFHC [38]. The single-mode optical fiber cladding thickness on the surface of the OFHC is on the order of a micrometer. A single crystal silicon microsphere with a radius of approximately $a = 500$ μm and refractive index 3.5 is

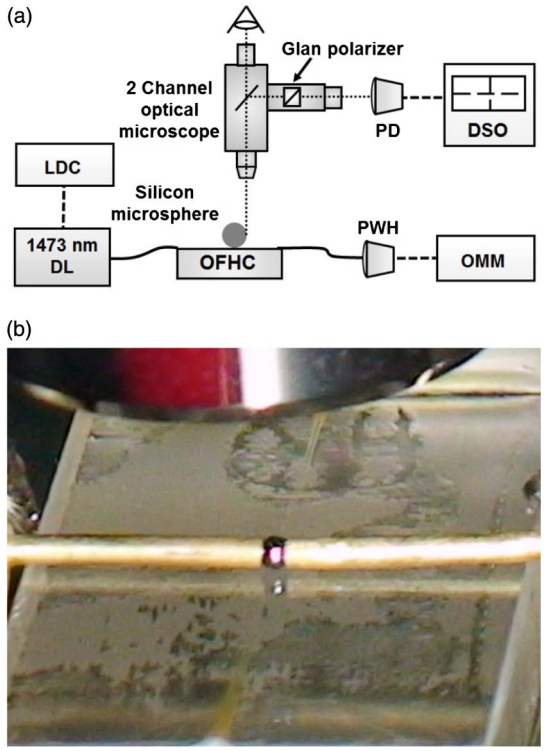


Fig. 3. (a) Schematic of the experimental setup describing the elastic scattering from the silicon microsphere. (b) Picture of the silicon microsphere positioned on the silica OFHC.

placed on the OFHC. The silicon microsphere is produced by the solidification of molten silicon melt and purified to a high level [39]. Then the silicon microsphere is lapped and polished mechanically to make a mirror-like finish with no surface deformations [40]. The silicon microsphere has approximately 2% ellipticity, which can result in WGM degeneracy.

In order to tune the wavelength of the DL, the temperature of the DL is controlled using a laser diode controller (LDC). The temperature of the DL is tuned from 14°C to 16.2°C at a constant operating DL current of 26.3 mA. That temperature range of 14°C to 16.2°C corresponds to a wavelength range of 1472.56–1473.42 nm. The elastically scattered light from the silicon microsphere at 90° is collected by a two-channel optical microscope and detected by an InGaAs photodiode (PD). The elastically scattered light is separated by a beam splitter placed at an angle of 45° with respect to the collected beam. The polarization of the collected light is controlled with a Glan polarizer, which is inserted before the InGaAs PD. The InGaAs PD signal is sent to a digital storage oscilloscope (DSO) for signal monitoring and data acquisition. An optical multimeter (OMM) with an InGaAs power wave head (PWH) is used to monitor the wavelength and power of the transmitted signal. All the optoelectronic equipments are controlled using the general-purpose interface bus standard.

5. EXPERIMENTAL RESULTS AND ANAYSIS

Figure 4(a) shows a spectrum of the elastically scattered (detected without a Glan polarizer) light from the silicon microsphere. Figures 4(b) and 4(c) present the spectra of the elastically scattered light with a Glan polarizer in the detection path (as shown in Fig. 3). The $\Delta\lambda$ of the WGMs is observed to

be 0.27 nm, which agrees well with the $\Delta\lambda$ estimated using Eq. (1) for a 1 mm diameter silicon microsphere with refractive index of 3.5.

As we are using an OFHC made from a single-mode optical fiber with a core radius of 2 μm, typical mode numbers (n) are on the order of the size parameter $x = 2000$. These 2000 degenerate modes cover a polar angular distribution of $\pi/2$ radians. For a 500 μm radius sphere, the polar angular coverage of the fiber corresponds to $2/500 = 0.004$ rad, which corresponds to a WGM degeneracy of 5. However, using the ellipticity Eq. (3), for our silicon microsphere with approximately 2% ellipticity, the WGM shifts are from 5 to 10 nm. Assuming a degeneracy of approximately 2000, the minimum degenerate mode spacing is approximately $5/2000$ nm $= 0.0025$ nm, which is on the order of our DL linewidth $\delta\lambda_{\text{laser}} = 0.0015$ nm; therefore we might not be able to discriminate between degenerate WGMs.

Using the mode density from Eq. (2), the total number of resonances is estimated to be approximately 18,000 for the spectral range (0.83 nm) covered in Figs. 4(a), 4(b), and 4(c). The observed number of WGMs in Figs. 4(a), 4(b), and 4(c) is approximately 450, which is only 2.5% of the all available resonances. The number of observed resonances is limited by the quality factor of the laser $Q_{\text{laser}} = \lambda_{\text{laser}}/\delta\lambda_{\text{laser}} = 1473/0.0015 = 10^6$. Additionally, due to the localization principle [35], only the WGMs at the right impact parameter b are excited efficiently by the input Gaussian beam in the OFHC. Also, because of the high refractive index (3.5) of Si, the propagation constant k mismatch, leading to

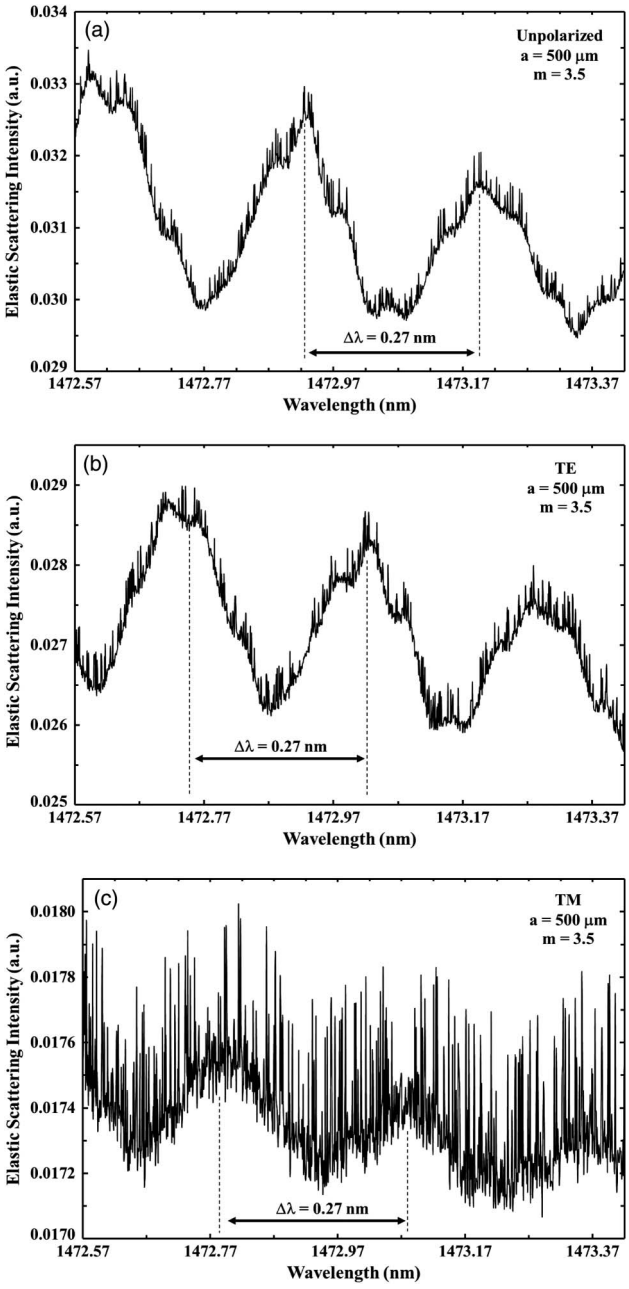


Fig. 4. Elastic scattering intensity (a) unpolarized, (b) TE polarized, and (c) TM polarized spectra from a silicon microsphere.

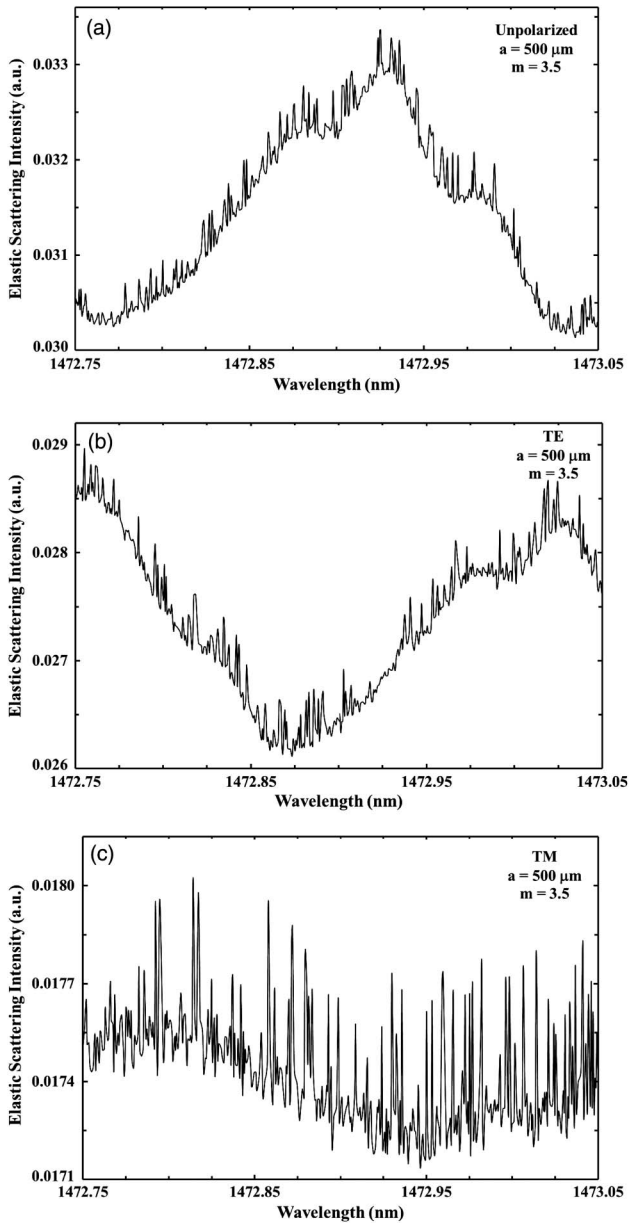


Fig. 5. Single-mode spacing ($\Delta\lambda$) spectral coverage for (a) unpolarized, (b) TE polarized, and (c) TM polarized elastic scattering from a silicon microsphere.

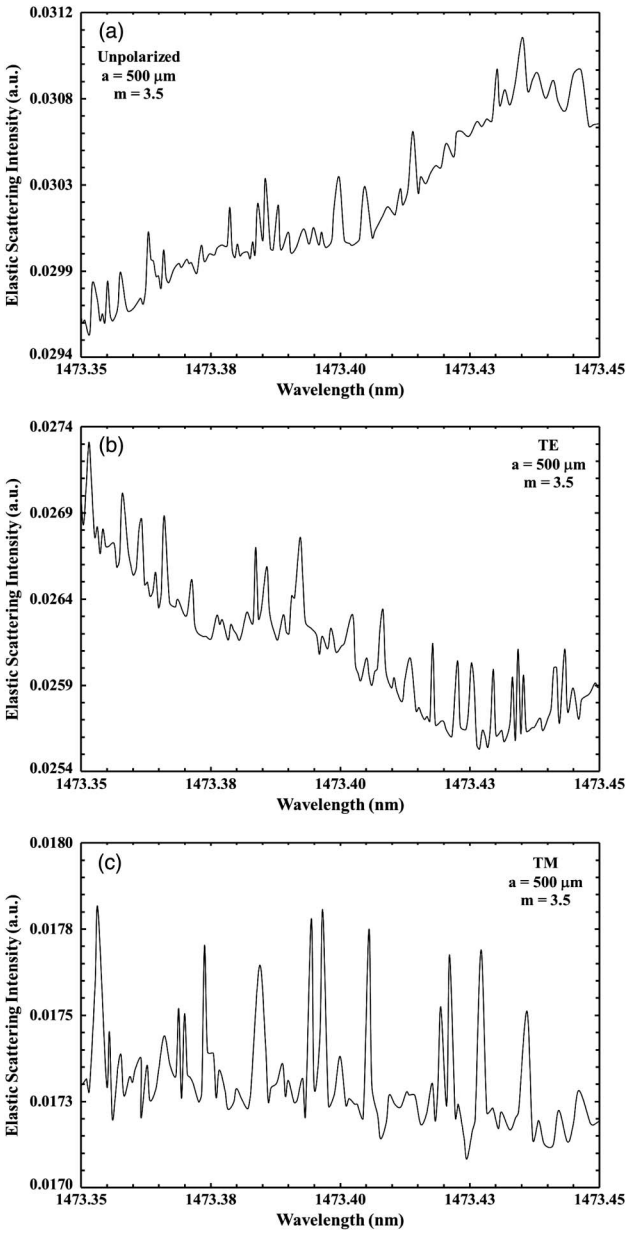


Fig. 6. One-third of mode spacing ($\Delta\lambda/3$) in spectral coverage for (a) unpolarized, (b) TE polarized, and (c) TM polarized elastic scattering from a silicon microsphere.

phase mismatch [36], between the OFHC and the silicon microsphere degrades the coupling to some WGMs.

The BG and the MD in Figs. 4(a), 4(b), and 4(c) are due to the interference of elastic scattering contributions from the WGMs, the OFHC SIs, and the GS [41]. As expected for the TM polarization, there is less BG and MD in the spectrum of Fig. 4(c) when compared to the BG and MD in the unpolarized and the TE polarized spectra in Figs. 4(a) and 4(b), since there is less TM-polarized SI scattering.

Figures 5(a), 5(b), and 5(c) zoom in to a single-mode spacing $\Delta\lambda$ spectral region of Figs. 4(a), 4(b), and 4(c), respectively. The occurrence of closely spaced resonances in the spectra of Fig. 5 is the result of the large optical size of the silicon microsphere. Figures 6(a), 6(b), and 6(c) zoom in to a third mode spacing $\Delta\lambda/3$ spectral region of Figs. 4(a), 4(b), and 4(c), respectively. The linewidths of the WGMs in the figures are found to be of the order of 10^{-3} nm, which corresponds to quality factors $Q = \lambda/\delta\lambda$ on the order of 10^6.

6. CONCLUSIONS

The polarization behavior of the 90° elastic light scattering spectra from a silicon microsphere with a radius of 500 μm and a refractive index of 3.5 is analyzed in the near-infrared S-band. The spectral mode spacing of the WGMs is observed to be 0.27 nm, which correlates well with the optical size of the silicon microsphere. The spectral linewidths of the WGMs are on the order of 10^{-3} nm, which corresponds to quality factors on the order of 10^6. The TE and TM WGMs can be detected selectively with the use of a Glan polarizer. The TE and TM polarization selectivity provides the ability to select relative WGM to MD or to BG levels. The TM polarization provides higher WGM signal levels with respect to MD and BG and is suitable for optical monitoring, sensing, or any other optoelectronic application that requires a high-resolution optical filter.

ACKNOWLEDGMENTS

This work was supported in part by the Türkiye Bilimsel ve Teknolojik Araştırma Kurumu (TÜBİTAK) grant no. EEEAG 106E215 and European Commission grants nos. FP6-IST-003887 NEMO and FP6-IST-511616 PHOREMOST.

REFERENCES

1. N. Hauke, A. Tandaechanurat, T. Zabel, T. Reichert, H. Takagi, M. Kaniber, S. Iwamoto, D. Bougeard, J. J. Finley, G. Abstreiter, and Y. Arakawa, "A three-dimensional silicon photonic crystal nanocavity with enhanced emission from embedded germanium islands," New J. Phys. **14**, 083035 (2012).
2. B. Charbonnier, S. Menezo, P. O'Brien, A. Lebreton, J. M. Fedeli, and B. Ben Bakir, "Silicon photonics for next generation FDM/FDMA PON," J. Opt. Commun. Netw. **4**, A29–A37 (2012).
3. E. Kasper, M. Kittler, M. Oehme, and T. Arguirov, "Germanium tin: silicon photonics toward the mid-infrared," Photon. Res. **1**, 69–76 (2013).
4. A. V. Rylyakov, C. L. Schow, B. G. Lee, W. M. J. Green, S. Assefa, F. E. Doany, M. Yang, J. Van Campenhout, C. V. Jahnes, J. A. Kash, and Y. A. Vlasov, "Silicon photonic switches hybrid-integrated with CMOS drivers," IEEE J. Solid-State Circuits **47**, 345–354 (2012).
5. Y. Chen, Z. Li, H. Yi, Z. Zhou, and J. Yu, "Microring resonator for glucose sensing applications," Front. Optoelectron. China **2**, 304–307 (2009).
6. W. Bogaerts, P. De Heyn, T. Van Vaerenbergh, K. De Vos, S. Kumar Selvaraja, T. Claes, P. Dumon, P. Bienstman, D. Van Thourhout, and R. Baets, "Silicon microring resonators," Laser Photon. Rev. **6**, 47–73 (2012).
7. J. Ballato, T. Hawkins, P. Foy, R. Stolen, B. Kokuzo, M. Ellison, C. McMillen, J. Reppert, A. M. Rao, M. Daw, S. Sharma, R. Shori, O. Stafsudd, R. R. Rice, and D. R. Powers, "Silicon optical fiber," Opt. Express **16**, 18675–18683 (2008).
8. C.-F. Lin, S.-C. Hung, S.-C. Shiu, and H.-J. Syu, "Si micro and nano-structures for communication and energy applications," Proc. SPIE **8564**, 85640R (2012).
9. A. Serpengüzel and A. W. Poon, eds., *Optical Processes in Microparticles and Nanostructures: A Festschrift Dedicated to Richard Kounai Chang on His Retirement from Yale University* (World Scientific, 2011).
10. T. Bilici, S. Isçi, A. Kurt, and A. Serpengüzel, "Microsphere-based channel dropping filter with an integrated photodetector," IEEE Photon. Technol. Lett. **16**, 476–478 (2004).
11. X. Lu, J. Y. Lee, P. X.-L. Feng, and Q. Lin, "Silicon carbide microdisk resonator," Opt. Lett. **38**, 1304–1306 (2013).
12. J. Zhu, S. K. Ozdemir, Y.-F. Xiao, L. Li, L. He, D.-R. Chen, and L. Yang, "On-chip single nanoparticle detection and sizing by mode

splitting in an ultrahigh-*Q* microresonator," Nat. Photonics **4**, 46–49 (2009).
13. L. Jin, J. Wang, X. Fu, B. Yang, Y. Shi, and D. Dai, "High-*Q* microring resonators with 2 × 2 angled multimode interference couplers," IEEE Photon. Technol. Lett. **25**, 612–614 (2013).
14. A. Demir, E. Yüce, A. Serpengüzel, and J. A. Lock, "Geometrically enhanced morphology dependent resonances of a dielectric sphere," Appl. Opt. **50**, 6652–6656 (2011).
15. H. Agha, J. E. Sharping, M. A. Foster, and A. L. Gaeta, "Optimal sizes of silica microspheres for linear and nonlinear optical interactions," Appl. Phys. B **83**, 303–309 (2006).
16. Y. Hu, L. Zhang, X. Xiao, Z. Li, Y. Li, T. Chu, Y. Su, Y. Yu, and J. Yu, "An ultra-high-speed photonic temporal differentiator using cascaded SOI microring resonators," J. Opt. **14**, 065501 (2012).
17. K. Xu, G. K. P. Lei, S. M. G. Lo, Z. Cheng, C. Shu, and H. K. Tsang, "Bit-rate-variable DPSK demodulation using silicon microring resonators with electro-optic wavelength tuning," IEEE Photon. Technol. Lett. **24**, 1221–1223 (2012).
18. C. Sang-Yeon, G. Dobbs, N. M. Jokerst, B. Mizaikoff, and T. Cooper, "Optical microring resonator sensors with selective membrane surface customization," in *Proceedings of the Conference on Lasers and Electrooptics/Quantum Electronics and Laser Science Conference and Photonic Applications Systems Technologies 2007*, Technical Digest (OSA, 2007), paper CWE4.
19. U. Woggon, R. Wannemacher, M. V. Artemyev, B. Möller, N. Lethomas, V. Anikeyev, and O. Schöps, "Dot-in-a-dot: electronic and photonic confinement in all three dimensions," Appl. Phys. B **77**, 469–484 (2003).
20. J. Ward and O. Benson, "WGM microresonators: sensing, lasing and fundamental optics with microspheres," Laser Photon. Rev. **5**, 553–570 (2011).
21. Y. O. Yılmaz, A. Demir, A. Kurt, and A. Serpengüzel, "Optical channel dropping with a silicon microsphere," IEEE Photon. Technol. Lett. **17**, 1662–1664 (2005).
22. E. Xifré-Pérez, J. Domenech, R. Fenollosa, P. Muñoz, J. Capmany, and F. Meseguer, "All silicon waveguide spherical microcavity coupler device," Opt. Express **19**, 3185–3192 (2011).
23. X. Li, A. Pyatenko, Y. Shimizu, H. Wang, K. Koga, and N. Koshizaki, "Fabrication of crystalline silicon spheres by selective laser heating in liquid medium," Langmuir **27**, 5076–5080 (2011).
24. P. Wang, T. Lee, M. Ding, A. Dhar, T. Hawkins, P. Foy, Y. Semenova, Q. Wu, J. Sahu, G. Farrell, J. Ballato, and G. Brambilla, "Germanium microsphere high-*Q* resonator," Opt. Lett. **37**, 728–730 (2012).
25. E. Yüce, O. Gürlü, and A. Serpengüzel, "Optical modulation with silicon microspheres," IEEE Photon. Technol. Lett. **21**, 1481–1483 (2009).
26. H. Yılmaz and A. Serpengüzel, "Electro-optical modulation with silicon microspheres in liquid crystal," Proc. SPIE **8069**, 80690L (2011).
27. A. Y. Smirnov, S. N. Rashkeev, and A. M. Zagoskin, "Polarization switching in optical microsphere resonator," Appl. Phys. Lett. **80**, 3503–3505 (2002).
28. G. Guan and F. Vollmer, "Polarized transmission spectra of the fiber–microsphere system," Appl. Phys. Lett. **86**, 121115–121117 (2005).
29. H. Konishi, H. Fujiwara, S. Takeuchi, and K. Sasaki, "Polarization-discriminated spectra of a fiber–microsphere system," Appl. Phys. Lett. **89**, 121107–121109 (2006).
30. S. Götzinger, L. de S. Menezes, O. Benson, D. V. Talapin, N. Gaponik, H. Weller, A. L. Rogach, and V. Sandoghdar, "Confocal microscopy and spectroscopy of nanocrystals on a high-*Q* microsphere resonator," J. Opt. B **6**, 154–158 (2004).
31. P. Chylek, "Resonance structure of Mie scattering: distance between resonances," J. Opt. Soc. Am. A **7**, 1609–1613 (1990).
32. S. C. Hill and R. E. Benner, "Morphology-dependent resonances," in *Optical Effects Associated with Small Particles*, P. W. Barber and R. K. Chang, eds. (World Scientific, 1998), pp. 3–61.
33. S. Arnold, "Microspheres, photonic atoms and the physics of nothing," Am. Scientist **89**, 414–421 (2001).
34. H. M. Nussenzveig, "Complex angular momentum theory of the rainbow and the glory," J. Opt. Soc. Am. A **69**, 1068–1079 (1979).
35. M. Cai, O. Painter, and K. J. Vahala, "Observation of critical coupling in a fiber taper to a silica-microsphere whispering-gallery mode system," Phys. Rev. Lett. **85**, 74–77 (2000).
36. G. Chen, M. M. Mazumder, Y. Chemla, A. Serpengüzel, R. Chang, and S. Hill, "Wavelength variation of laser emission along the entire rim of slightly deformed microdroplets," Opt. Lett. **18**, 1993–1995 (1993).
37. W. T. Grandy, *Scattering of Waves from Large Spheres* (Cambridge University, 2000).
38. O. Parriaux, S. Gidon, and A. A. Kuznetsov, "Distributed coupling on polished single-mode optical fibers," Appl. Opt. **20**, 2420–2423 (1981).
39. W. R. McKee, "Development of the spherical silicon solar cell," IEEE Trans. Comp. Hybrids Manufact. Technol. **5**, 336–341 (1982).
40. N. Takeda, "Spherical silicon 1 mm device and its clustering," in *Proceedings of the IEEE International Symposium on Advanced Packaging Materials: Processes, Properties and Interfaces* (IEEE, 2001), pp. 86–91.
41. A. Serpengüzel, S. Arnold, G. Griffel, and J. A. Lock, "Enhanced coupling to microsphere resonances with optical fibers," J. Opt. Soc. Am. B **14**, 790–795 (1997).